

Electrical Rectification by a Monolayer of Hexadecylquinolinium Tricyanoquinodimethanide Measured between Macroscopic Gold Electrodes

Robert M. Metzger,* Tao Xu, and Ian R. Peterson†

Laboratory for Molecular Electronics, Chemistry Department, The University of Alabama, Tuscaloosa, Alabama 35487-0336

Received: March 22, 2001

Unimolecular rectification was detected between oxide-free Au electrodes for a Langmuir–Blodgett (LB) monolayer of the zwitterionic $D^+-\pi-A^-$ molecule hexadecylquinolinium tricyanoquinodimethanide, $C_{16}H_{33}Q-3CNQ$. The top gold pad was deposited by a process that cools the metal vapor before deposition. The maximum rectification ratio is 27.5 at 2.2 V (the average rectification ratio is 7.55). The currents are as large as 9.04×10^4 electrons molecule $^{-1}$ s $^{-1}$. The result reinforces previous work with oxide-bearing Al electrodes, but the currents with Au electrodes are larger by 3–5 orders of magnitude. Rectification was also seen for a nine-monolayer Z-type LB film between similar Au electrodes but not for a monolayer of arachidic acid. The direction of enhanced electron current is from the negatively charged dicyanomethylene end of $C_{16}H_{33}Q-3CNQ$ to the quinolinium ring, as predicted by the Aviram–Ratner analysis. However, there is a good fit to the behavior expected for quantum conduction dominated by a single molecular level. The best-fit energy for this level is 1.31 ± 0.25 eV above the Fermi level of the Au electrode.

Introduction

Langmuir–Blodgett (LB) monolayers and multilayers of the ground-state zwitterionic donor- π -acceptor ($D^+-\pi-A^-$) molecule hexadecylquinolinium tricyanoquinodimethanide ($C_{16}H_{33}Q-3CNQ$, **1**) were first reported by Sambles, Ashwell, and co-workers to be electrically rectifying between a Pt electrode on one side and a Mg pad (protected by Ag) on the other side¹ and also with intervening monolayers of insulating aliphatic acids.² The rectification was confirmed conclusively with Al electrodes on *both* sides of monolayers and multilayers.³ The mechanism of rectification was explained,³ and it was suggested that the highest occupied molecular orbital (HOMO) and the lowest unoccupied molecular orbital (LUMO) of **1** were involved in the enhanced current observed in the forward direction.³ Most junctions rectify as described, but some cells are symmetrical, and some rectify (with much lower currents) in the opposite direction.⁴ The rectification was measured in the temperature range 370–105 K with no definite temperature dependence.⁵ Spectroscopic and electrochemical data confirmed the zwitterionic ground state and the much less polar first excited state.⁶

The large enhancement in the forward current was ascribed to resonance between the Fermi level of the Al electrodes, appropriately shifted by the applied electrical potential, and the LUMO of the molecule.³ The relaxation of the molecule after electron transfer is most likely associated with the intervalence transfer band, which is measured at 570 nm (2.17 eV) in films of **1**, between the ground state (dipole moment 43 ± 8 D)³ and the first electronic excited state (dipole moment between 3 and 9 D).⁶ The results have been reviewed extensively.^{7–15}

A persistent question was whether the defective oxide covering of Al or Mg, unavoidably present on both sides of the

organic monolayer, was in any way involved in the rectification process, besides limiting the total current through the device.^{13–15} We now show that rectification occurs also when monolayers or multilayers of **1** are placed between oxide-free gold electrodes. A preliminary report of our new work with Au electrodes has been presented elsewhere.¹⁶

Electrical Conduction through Thin Films

After several decades of work on electrical conduction across thin films sandwiched between metal electrodes, Bethe¹⁷ obtained an expression for quantum-mechanical tunneling across a barrier,¹⁷ which predicts ohmic (linear) variation of the current with the voltage at low biases and superlinear behavior at higher voltages. Mann and Kuhn fabricated monolayer cells with evaporated top metal contacts.¹⁸ As a result of the fits of their measured values of current and voltage to the Bethe law, these researchers claimed that many of their cells were defect-free. Unfortunately, Mann and Kuhn used aluminum as the top-contact metal, with its inescapable layer of insulating native oxide. It was first shown for such cells by Vincett and Roberts,¹⁹ and then in greater detail by Tredgold et al.,²¹ that the logarithm of the current varies essentially linearly with the fourth root of voltage over several decades of current. This $\log I$ versus $V^{0.25}$ relationship has as yet received no satisfactory theoretical explanation, but experimental evidence connects it to nanofilaments of top-contact metal²¹ penetrating as far as the native oxide. The nanofilaments do not penetrate the monolayer at random but are associated with structural point defects.²²

While theory gives no basis for $\log I$ versus $V^{0.25}$, there are a number of known mechanisms in which the logarithm of the current varies linearly with a power of the voltage. In a pn-junction rectifier, the carriers must cross a single barrier, and $\log I$ varies linearly with V . In the well-known Poole–Frenkel mechanism, carriers must continually escape across the potential barriers surrounding the traps which capture them,²³ and $\log I$

* To whom correspondence should be addressed.

† Permanent address: Centre for Molecular & Biomolecular Electronics, Department of Natural & Environmental Sciences, University of Coventry, Priory Street, Coventry CV1 5FB, United Kingdom.

varies as $V^{0.50}$. None of the above laws take into account the molecular structure of a monolayer.

For a single mode of a molecule linked to macroscopic metal electrodes, Landauer²⁴ and later Datta²⁵ have shown that the current I as a function of the bias V is

$$I(V) = (e/h) \int_{E=-\infty}^{E=\infty} \tau(E,V) \Delta p(E,V) dE \quad (1)$$

where e is the electronic charge, h is Planck's constant, $\Delta p(E,V)$ is the difference in the Fermi–Dirac occupation factors of the levels at energy E in the electrodes on the two sides, and $\tau(E,V)$ is the transmission factor. If the transmission factor $\tau(E,V)$ is unity (it is usually less than that), the molecule can be considered to be a nanowire. Equation 1 then yields a well-defined conductance $G = (e^2/h) = 38.8 \mu\text{S}$. For a spin-degenerate pair of modes, this corresponds to a resistance $R = (h/2 e^2) = 12.9 \text{ k}\Omega$. When the nanowire has several modes, whose propagating energy range straddles the Fermi level, each one contributes $38.8 \mu\text{S}$ to the total conductance.

In light of all of the above, the following equations have been considered for fitting the data acquired in this study: a simple exponential,

$$I = a \exp(bV) \quad (2)$$

a Poole–Frenkel curve,²³

$$I = a' \exp(b'V^{0.5}) \quad (3)$$

a Tredgold–Roberts curve,^{19,20}

$$I = a'' \exp(b''V^{0.25}) \quad (4)$$

the Bethe–Sommerfeld tunneling equation,¹⁷

$$I = a'''V^{0.5} \exp(-b'''V^{0.5}) \quad (5)$$

an equation derived by Hush and co-workers²⁶ for a single atom of energy E placed symmetrically between two metal electrodes of Fermi level E_F and subjected to a bias,

$$I = (4e\Delta/h) \{ \tan^{-1}[(E_F - E + eV/2)/2\Delta] - \tan^{-1}[(E_F - E - eV/2)/2\Delta] \} \quad (6a)$$

$$I = a'''' \{ \tan^{-1}[b''''(c + V)] - \tan^{-1}[b''''(c - V)] \} \quad (6b)$$

where Δ is the imaginary component of the self-energy, and a similar equation proposed by Peterson et al. for the case of molecular conduction dominated by a single level,²⁷

$$I = I_0 \{ \tan^{-1}[\theta(E_0 + p eV)] - \tan^{-1}[\theta(E_0 - (1 - p)eV)] \} \quad (7)$$

where p is the fractional position of the “center of gravity” of the relevant molecular orbital between the two electrodes, E_0 is the energy of the molecule above the Fermi level of the electrode, I_0 is the saturation value of the resonant tunneling current, and θ is a tunneling gap coupling parameter.

While the Aviram–Ratner model of rectifier behavior predicts a current plateau beyond a threshold bias in the forward direction, as do eqs 6 and 7, the other models (eqs 2–5) have no plateau but imply a continuous increase of current, presumably, until irreversible dielectric breakdown is achieved. Therefore, it is of some interest to probe, with the Au electrodes, which equation best fits the experimental results.

For the work reported below, the rectification ratio $RR(V)$ at a bias V is defined as the ratio of the current I at a forward bias V , divided by the current $-I'$ at the corresponding negative bias $-V$:

$$RR = I(V)/-I'(-V) \quad (8)$$

Experimental Details

It is easy to transfer one or more monolayers onto a metal electrode, but it is not simple to deposit a metal layer atop an organic layer without damaging it. Sambles' original method used Mg vapor, which, in his experience, damaged an organic film the least.^{1,2} Our improvement³ was to cryocool the “glass|Al|LB film” assembly to 77 K and thus prevent, or at least reduce, thermal damage to the organic film when Al vapor condenses on top of it, to form the “glass|Al|LB film|Al” assembly.^{3,28} When Au vapor was used in our laboratory, the cryocooling of the substrate was ineffective: the organic layer was destroyed by the hot Au vapor. Recently, Okazaki and Sambles showed that, by introducing a low pressure of Ar (4×10^{-3} Torr) into the evaporator during Au vapor deposition, and by blocking by baffles a direct path from the Au source to the target, only Au atoms that had scattered off Ar atoms several times could reach the organic multilayer of arachidic acid.³¹

The procedure of Okazaki and Sambles was implemented successfully in our laboratory for a monolayer of **1**, as reported recently.¹⁶ We present here the full details of our procedure.

Five substrates with multiple pads each were studied; we shall call them samples A, B, C, D, and E. Two samples of Corning glass, labeled A and B, 50 mm \times 50 mm \times 0.4 mm, with rms roughness of 2.3 Å (measured by X-ray reflectivity) were washed with 2-propanol and then with xylene. Fifty nanometers of Au was evaporated onto the hydrophobic glass from a Mo boat in an Edwards E306 evaporator. Although no Cr underlayer was used for samples A and B, rendering the glass surface hydrophobic with xylene prevented the subsequent detachment of the Au from the glass surface during work in the film balance or Langmuir trough.

Samples C, D, and E were glass substrates (50 mm \times 50 mm \times 0.4 mm) onto which a 20-nm Cr underlayer was sputtered using a Vac-Tec Model 250 batch side-sputtering system (the deposition power was 200 W, the Ar pressure was 5 mTorr, and the base pressure was 2.4×10^{-7} Torr). The Cr underlayer was covered by a 50-nm thick Au layer evaporated in the Edwards evaporator.

Additional samples were also prepared for characterization of the monolayer by grazing-angle X-ray diffraction, ellipsometry, and grazing-angle infrared absorption spectroscopy. All glass/Si substrates were cleaned first with acetone for 2 min and then with 2-propanol for 2 min in an ultrasonic bath. Evaporator vacuum is below 4×10^{-6} mbar. Ten nanometers of Cr was evaporated as an adhesion layer, and 150 nm of Au was then evaporated on top of the Cr layer. The sample was then taken out of the vacuum chamber, cleaned by UV-ozone for 80 s, and immersed into deionized water immediately. A LB monolayer was then deposited on the upstroke onto the gold surface at the water–air interface at 12 °C. The surface pressure was 25 mN/m⁻¹. The transfer ratio was slightly above 100%. The sample was then dried in a vacuum above P₂O₅ for 72 h before X-ray, ellipsometry, or grazing-angle infrared absorption measurements.

Grazing-angle X-ray diffraction was performed on a Philips X'pert diffractometer in the Bragg–Brentano (θ – 2θ) geometry, using Ni-filtered line-focused Cu K α radiation [$\lambda(K_{\alpha 1}) =$

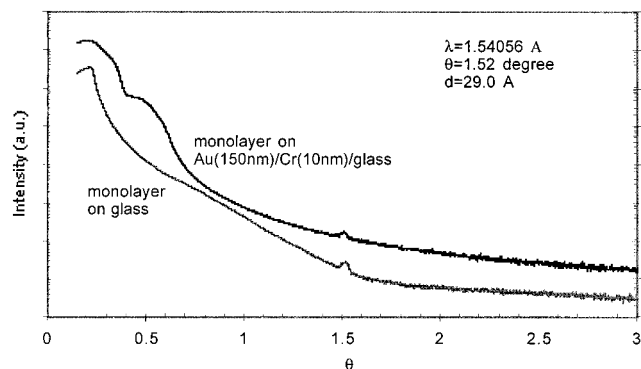


Figure 1. X-ray diffractograms of a LB monolayer of **1** on glass and on Au. A single peak at Bragg angle $\theta = 1.52^\circ$ (monolayer film thickness of 29.0 Å) can be seen for both glass and Au substrates.

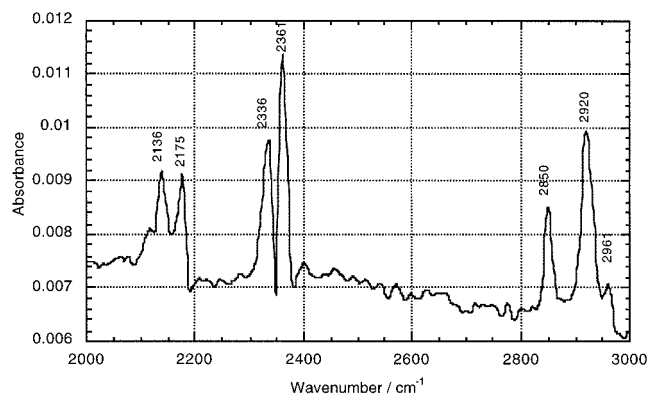


Figure 2. Grazing-incidence infrared absorption spectrum (angle of incidence 80°) of monolayer of **1** on Au. The peaks at 2336 and 2361 cm^{-1} are due to CO_2 (imperfect purging of chamber). The features at 2850, 2920, and 2961 cm^{-1} are CH_2 scissor modes. The peak at 2136 cm^{-1} is due to a $\text{C}\equiv\text{N}$ stretch ("neutral" CN group), while the peak at 2175 cm^{-1} is due to a $\text{C}\equiv\text{N}$ stretch (negatively charged CN group).

1.540 56 Å] in the incident angle range $\theta = 0.15\text{--}3^\circ$ (Figure 1). A graded parabolic focusing mirror was used to transform a divergent X-ray beam into a quasi-parallel incident beam with angular divergence of about 0.05° . Before each measurement, the sample was carefully aligned.²⁹

Ellipsometric measurements were carried out in a Woolam spectroscopic ellipsometer in the range 750–1000 nm (where the molecule absorbs weakly³), using three different angles of incidence (65° , 70° , and 75°); the measured polarization angles Δ and Ψ were measured for both a Au substrate (probably bearing a layer of impurities adsorbed from the laboratory atmosphere) and the Au film bearing a single monolayer of $\text{C}_{16}\text{H}_{33}\text{Q}-3\text{CNQ}$ above clean Au.

The grazing-incidence infrared spectrum of the monolayer on Au was obtained in a Bruker IFS-88 Fourier transform infrared spectrometer, using a Specac grazing-angle accessory and an Al wire grid polarizer. The grazing angles were 60, 70, and 80° , and the spectrum was ratioed to a monolayer-free Au reference (Figure 2).

To ensure that the Au surface stayed hydrophilic, all samples were immediately placed under pure water (resistivity = 18 MΩ cm) and left under water until a monolayer (for samples A and C; or a nine-layer multilayer, for sample B) of freshly prepared $\text{C}_{16}\text{H}_{33}\text{Q}-3\text{CNQ}$ (**1**) was transferred (Z-type, with transfer ratios of 100% or even more) from a monolayer of $\text{C}_{16}\text{H}_{33}\text{Q}-3\text{CNQ}$ at the air–water interface held at a surface pressure of 25 mN/m in a NIMA model 622 film balance at 12 °C in a darkened HEPA-filtered room. A single monolayer of arachidic acid,

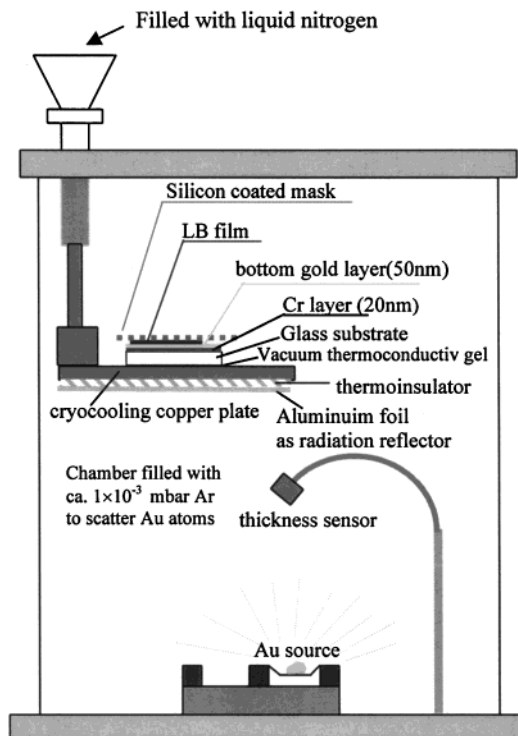


Figure 3. Geometry of evaporation.

$\text{C}_{19}\text{H}_{39}\text{COOH}$ (Aldrich), was deposited at pH 7 onto sample D. As before,³ the four samples coated by the LB layers were then dried individually in a vacuum desiccator over P_2O_5 for 3 days, to remove any entrapped water between the layers.

Two hydrophobic contact masks were prepared from a phenolic resin. After gross asperities were removed by polishing, the masks were coated with a $\sim 50\text{-}\mu\text{m}$ thick layer of partially methoxylated poly(dimethylsiloxane) resin (General Electric catalog no. GE 5060) by immersion in 3% w/w solution in toluene, followed by removal of excess liquid and evaporation of the solvent on a perfectly level surface.

Samples A, C, E (with a single monolayer of $\text{C}_{16}\text{H}_{33}\text{Q}-3\text{CNQ}$), B (bearing 9 monolayers of $\text{C}_{16}\text{H}_{33}\text{Q}-3\text{CNQ}$), and D (with a single monolayer of arachidic acid) were placed successively in the Edwards evaporator, atop a Cu cryosurface. Figure 3 shows the geometry of the evaporator, boat, and sample holder. The samples faced away from the boat. The cryosurface was cooled to 77 K using liquid nitrogen. For samples C, D, and E, a thermally conducting high-vacuum polymer gel (Mung II, Commonwealth Scientific Corp.) was applied between the glass substrate and the Cu cryotip, to improve the cryocooling effect. For samples C, D, and E, a sheet of thermally insulating polymer was placed between the cryotip and a layer of aluminum foil, which faced the evaporation boat, so that much of the radiant heat from the boat was dissipated beneath and away from the Cu cryotip (this is not shown in Figure 3). Gold was evaporated from a Mo boat under an Ar pressure of between 8×10^{-4} and 2×10^{-3} mbar, at a rate of 0.02 nm s^{-1} for the first 200 nm and then 0.1 nm s^{-1} for the next 400 nm, until the quartz thickness monitor recorded a nominal Au thickness of 600 nm. The Au pads that formed through the holes in the mask were much thinner than the nominal thickness of 600 nm: they were measured to be 17 nm thick (Sloan Dektak II profilometer); most of the evaporated Au deposited elsewhere inside the bell jar. The rms roughness was measured by atomic force microscopy (National Instruments Dimension 3000 scanned probe microscope) as 1 nm for the top of a Au pad and 0.4 nm for the

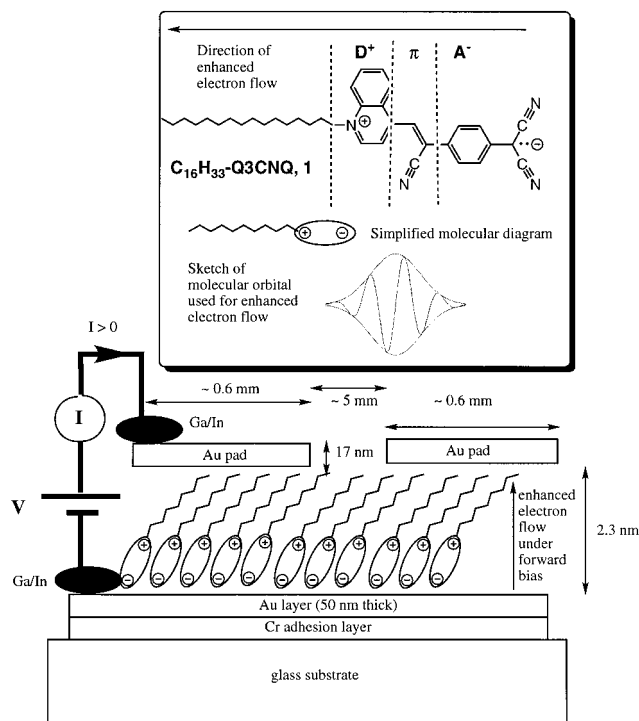


Figure 4. Side view of LB monolayer of **1** sandwiched between Au electrodes (two adjacent Au pads are shown; pad area 0.283 mm²) and electrical contacts attached to the Au. The direction of enhanced electron flow is shown. Inset: Chemical structure of ground-state zwitterionic molecule C₁₆H₃₃Q-3CNQ, **1**, its equivalent "tadpole" diagram, sketch of the molecular orbital involved in enhanced electron transfer, and direction of the enhanced electron flow relative to the long molecular axis.

bottom Au layer. The pads are cylindrical, with a diameter of 0.6 mm and an area of 0.283 mm². For sample C, four thermal monitors (Tempilabel) were placed close to the sample; these would change colors if the temperature of the Au vapor exceeded 93, 107, 121, or 135 °C. No color change occurred at all, so the Au vapor temperature was below 93 °C. We are confident that our experimental procedures did not allow the formation of any gold oxide monolayer atop the Au electrodes.

For sample A (monolayer of C₁₆H₃₃Q-3CNQ), 2 cells were good, and 8 were shorts. For sample C (monolayer of C₁₆H₃₃Q-3CNQ), 48 pads were measured: 16 were rectifying, as explained below, 32 were short-circuited, and none showed the "reverse rectification" seen for some monolayers between Al layers in ref 4.

The measuring electronics were modified from the earlier procedure.³ The same voltage source (Hewlett-Packard model 3245A) and multimeter (Hewlett-Packard model 3245A) were connected by a National Instruments IEEE-488 GPIB interface board to a Gateway 2000 model P5-60 microcomputer. The computer control program was written using a Borland Delphi (Inprise Corp.) compiler. The multimeter, sample, and all signal lines, except for some low-impedance high-level lines, were enclosed in a Faraday cage of complex topology, whose boundaries included the metal cabinet of the multimeter, a 100 × 200 × 200 mm³ welded Al test box with an Al lid secured by four bolts, and the continuous shield of a 20-core shielded cable. For convenience, the cable and test box were connected via a 25-way D-type subminiature connector; continuity of the Faraday cage was achieved via the mating metal shells of the plug and sockets. The boundary of the Faraday cage was breached only at the rear of the multimeter, for the entry of the 110 V ac power leads and the voltage source lines. The Faraday

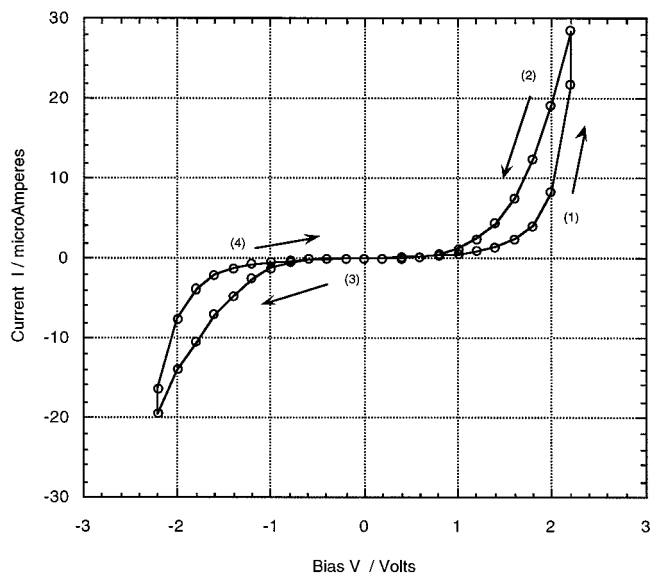


Figure 5. Current-voltage plot (I - V) for monolayer of arachidic acid, in cell "Au pad|monolayer of *n*-C₁₉H₃₉COOH|Au base" (sample D, pad aap2). Pad area = 0.283 mm². The arrows and numbers in parentheses show the measurement sequence. At 2.2 V, the resistance $R = 79$ k Ω , the current $I = 28.5$ μ A = 138 electrons molecule⁻¹ s⁻¹, and the nominal rectification ratio is RR = 1.47 (no rectification).

cage was grounded at this point and at no other. The test box was equipped with a magnetic baseplate, allowing convenient horizontal (X and Y) positioning of two Z -axis micropositioners secured to the baseplate by NdFeB magnets. Tinned flexible wires, controlled by the micropositioners, allowed contact to selected Au pads via a terminal droplet of Ga/In eutectic, which did not wet the gold. The efficacy of contact was estimated by eye.

Figure 4 shows the arrangement of the monolayer and the Au pads. The area per molecule was estimated as 50 Å²/molecule;³ the tilt angle of the molecule versus the normal to the surface was estimated as 45° from a direct measurement of the film thickness (2.3 nm) and the estimated molecular length.³

For each datum, the potential delivered by the HP 3245A source was reset, in increments of 0.2 V, by the computer program, and then the bias V and the current I were measured by the HP 3457A multimeter. The set and measured potentials were within 0.0001 V or less, unless $I > 1$ mA passed through the device; for 1 mA < I < 10 mA, the deviation was 0.001 V. When the current reached 136 mA, the device was short-circuited. All measurements were performed at room temperature.

Results

A single X-ray diffraction peak (Figure 1) from the monolayer was observed at Bragg angle $\theta = 1.52$ Å, corresponding to a monolayer film thickness of 29.0 Å (identical results on Au and on glass); from the full width at half-height of 0.037° (Au), that is, $\Delta\theta = 6.45 \times 10^{-4}$ rad, and the use of the Scherrer line-width equation $w = 0.89\lambda/\Delta\theta \cos \theta$,³⁰ a longitudinal correlation length $w = 2120$ Å can be deduced. No higher-order peaks were seen.

The measured ellipsometric polarization angles Δ and Ψ in the angular range 750–1000 nm were fitted by using a Cauchy expansion with $A = 1.38$ and $B = 0.01$. Using an assumed imaginary part of the refractivity $\kappa = 0.01$ (derived from the optical absorption³) and a slowly varying real part of the refractive index, the thickness was determined for five spots

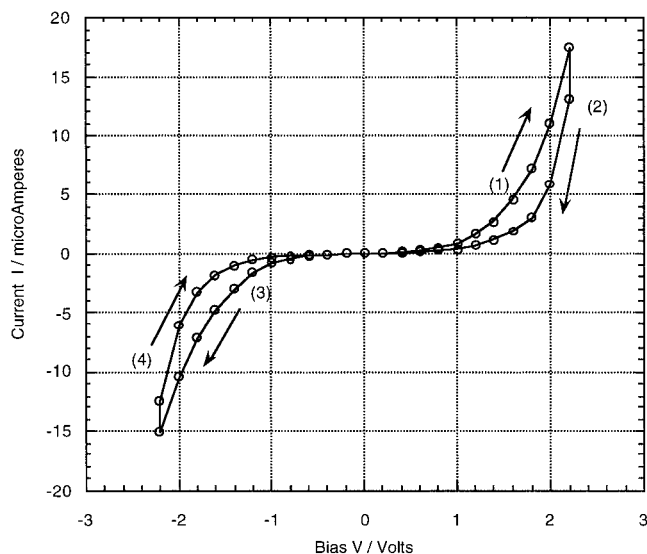


Figure 6. Current–voltage plot (I – V) for monolayer of arachidic acid in cell “Au pad|monolayer of n - $C_{19}H_{39}COOH$ |Au base” (sample D, pad aap3). Pad area = 0.283 mm^2 . The arrows and the numbers in parentheses show the measurement sequence. At $V = 2.2 \text{ V}$, the resistance $R = 130 \text{ k}\Omega$, the current $I = 17.38 \mu\text{A} = 84.3 \text{ electrons molecule}^{-1} \text{ s}^{-1}$, and the nominal rectification ratio $RR = 1.15$ (no rectification).

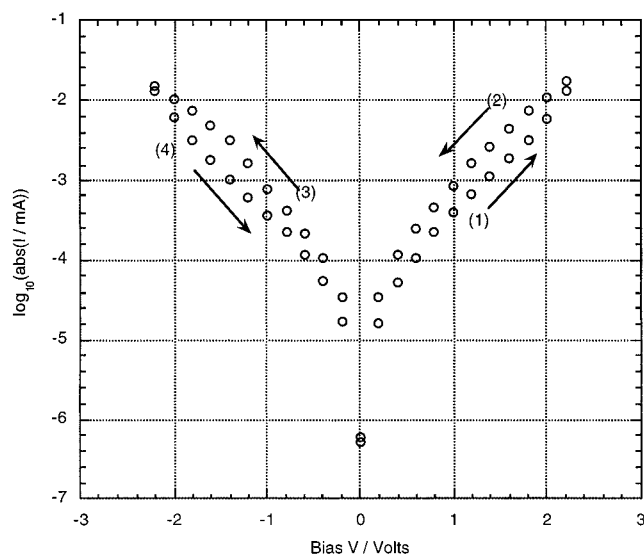


Figure 7. Logarithm of current versus voltage plot ($\log I$ – V), for monolayer of arachidic acid, in cell “Au pad|monolayer of n - $C_{19}H_{39}COOH$ |Au base” (sample D, pad aap3; same data as those used for Figure 6).

on the monolayer to be 22.44 ± 0.40 , 22.95 ± 0.43 , 22.77 ± 0.42 , 22.61 ± 0.39 , and $22.62 \pm 0.44 \text{ \AA}$; the average of these values was $22.7 \pm 0.4 \text{ \AA}$.

The grazing-incidence infrared spectrum (80°) is shown in Figure 2: it shows two broad peaks due to incomplete purging of CO_2 around 2300 cm^{-1} , CH_2 “scissor” peaks at 2961 , 2920 , and 2850 cm^{-1} , and two $\text{C}\equiv\text{N}$ stretch peaks at 2175 (negatively charged CN^3) and 2136 cm^{-1} (“neutral” CN^3).

Figures 5 and 6 show the results for arachidic acid (sample D). The curves show some hysteresis, as before,³ and a slight asymmetry, with rectification ratios $RR = 1.47$ and 1.15 , well below the threshold of $RR = 2.0$ previously set for significance.⁴ Figure 7 shows that the logarithm of the current is roughly linear with V past $\pm 0.4 \text{ V}$. Given that the pad areas are 0.283 mm^2 and the molecular areas are $22 \text{ \AA}^2 \text{ molecule}^{-1}$ (so there are 1.29

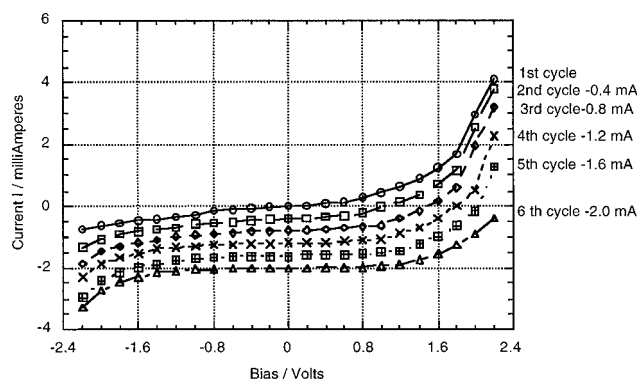


Figure 8. Current–voltage plots for six successive cycles of measurement for the same cell “Au pad|monolayer of $C_{16}H_{33}Q-3CNQ$ |Au base” (sample A, pad g1). For clarity, the data are displaced vertically downward by equal increments for the successive cycles. The bias is electrically grounded. At forward bias, positive current goes from the Au pad to the Au base (electrons flow from the Au base to the Au pad). Pad area = 0.283 mm^2 . At 2.2 V in the first cycle, the resistance $R = 538 \Omega$, the current $I = 4.09 \text{ mA} = 4.5 \times 10^4 \text{ electrons molecule}^{-1} \text{ s}^{-1}$, and the nominal rectification ratio $RR = 5.39$. RR decreases in successive cycles of measurement and disappears in cycle 6; RR becomes 4.52 , 3.84 , 3.16 , 2.13 , and 1.24 in cycles 2–6, respectively, as the forward (reverse) current decreases (increases) in magnitude.

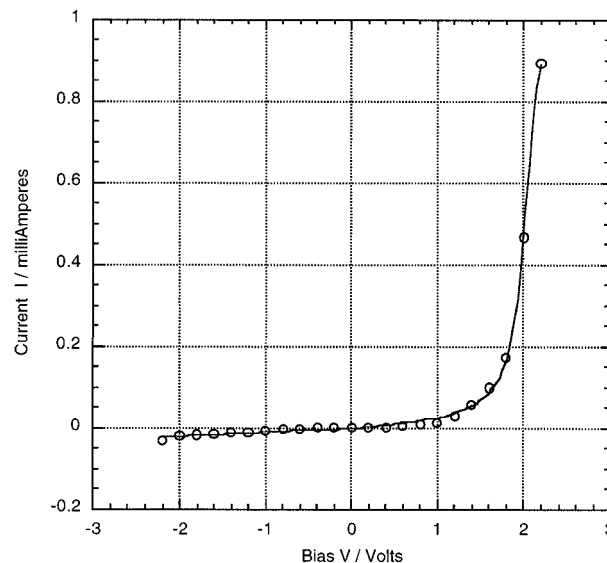


Figure 9. Current–voltage plot for the cell “Au pad|monolayer of $C_{16}H_{33}Q-3CNQ$ |Au base” (sample C, pad g3, first cycle). Pad area = 0.283 mm^2 . At 2.2 V , the resistance $R = 2.47 \text{ k}\Omega$, the current $I = 0.891 \text{ mA} = 9.83 \times 10^3 \text{ electrons molecule}^{-1} \text{ s}^{-1}$, and the rectification ratio for this first cycle $RR = 27.53$. RR decreases to 10.1 , 4.76 , 2.44 , and 1.86 in cycles 2–5, respectively, for the same pad. The solid line is the fit to eq 7, with $a = (6.42 \pm 0.11) \times 10^{-3} \text{ mA}$, $E_0 = 1.61 \pm 0.10 \text{ V}$, $p = 0.21 \pm 0.05$, $\theta = 9.64 \pm 0.86 \text{ V}^{-1}$, $r_p = 0.9996$, and $\chi^2 = 7.71 \times 10^{-4}$. The data for $V > 0$ can also be fit to eqs 2, 3, 4, 5, and 6, as given in Table 2. The data for $V < 0$ can also be fit separately to similar equations, with slightly lower r_p 's.

$\times 10^{12}$ molecules per pad), the maximum currents through a monolayer of arachidic acid at a bias of 2.2 V are 138 (Figure 5) and 84.3 (Figure 6) electrons molecule⁻¹ s⁻¹. It is expected that contact resistances will vary from sample to sample, in part because of differences in series resistance between the oxide-bearing tinned metal electrodes, the oxide-bearing Ga/In eutectic, and the oxide-free gold surface. The resistance at 2.2 V is $79 \text{ k}\Omega$ (Figure 5) or $130 \text{ k}\Omega$ (Figure 6). The arachidic acid data of Figures 5 and 6 can be fit to any one of eqs 2–7 with acceptable Pearson's $r_p > 0.995$,³² defined by

$$r_p = \frac{\sum_{i=1}^N (x_i - \langle x \rangle)(y_i - \langle y \rangle) [\sum_{i=1}^N (x_i - \langle x \rangle)^2]^{-1/2} [\sum_{i=1}^N (y_i - \langle y \rangle)^2]^{-1/2}}{\quad} \quad (9)$$

where x_i = observed value, y_i = calculated value, $\langle x \rangle$ = mean of observed values, and $\langle y \rangle$ = mean of calculated values. The fit parameters have moderate estimated standard errors, and they are not sufficiently close to each other to enable us to declare any of these fits superior to the others.

Figures 8–14 pertain to a single LB monolayer of $C_{16}H_{33}Q-3CNQ$ (1) sandwiched between Au electrodes, while Figure 15 shows the data for a nine-monolayer film of the same molecule placed between Au electrodes.

Figure 8 shows the results for the cell “Au pad|LB monolayer of $C_{16}H_{33}Q-3CNQ$ |Au base” (Run g1): the rectification lasts for six cycles, with the enhanced currents under positive bias

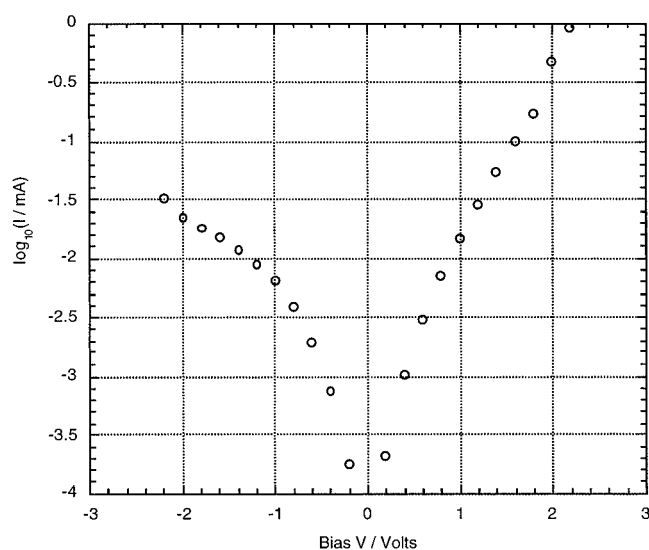


Figure 10. Logarithm of current versus voltage plot ($\log I-V$), for the cell “Au pad|monolayer of $C_{16}H_{33}Q-3CNQ$ |Au base” (sample C, pad g3, first cycle; same data as for Figure 9).

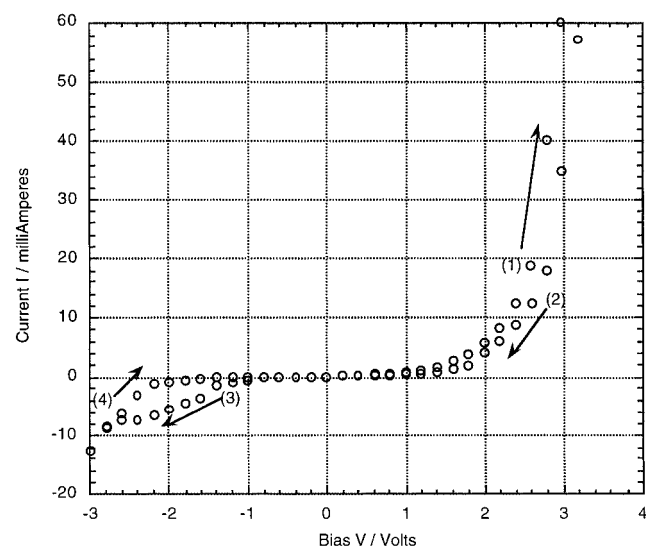


Figure 11. Current–voltage plots for the cell “Au pad|monolayer of $C_{16}H_{33}Q-3CNQ$ |Au base” (sample C, pad g24, first cycle). The arrows and the numbers in parentheses indicate the direction of bias sweep. Pad area = 0.283 mm^2 . At 2.2 V, the resistance $R = 0.268 \text{ k}\Omega$, the current $I = 8.20 \text{ mA} = 9.04 \times 10^4 \text{ electrons molecule}^{-1} \text{ s}^{-1}$, and the rectification ratio $RR = 6.62$. At 3.0 V, $I = 60.0 \text{ mA}$, and $RR = 4.75$.

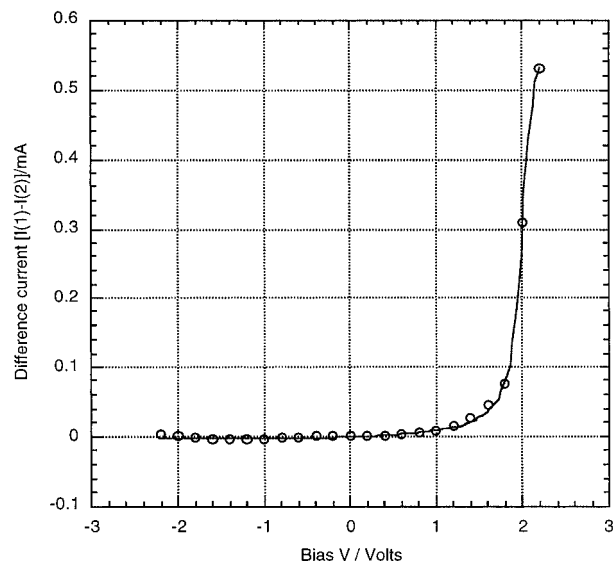


Figure 12. Difference current–voltage plot for the cell “Au pad|monolayer of $C_{16}H_{33}Q-3CNQ$ |Au base” (sample C, pad g3, first cycle minus second cycle). The solid line is the fit to eq 7, with $a = 0.202 \pm 0.003 \text{ mA}$, $E_0 = 2.54 \pm 0.57 \text{ V}$, $p = 0.27 \pm 0.27$, $\theta = 8.02 \pm 1.96 \text{ V}^{-1}$, and $r_p = 0.99972$.

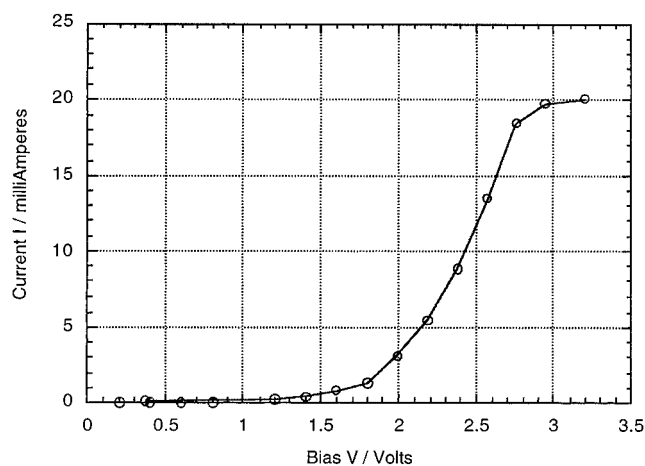


Figure 13. Current–voltage plot for the cell “Au pad|monolayer of $C_{16}H_{33}Q-3CNQ$ |Au base” driven until dielectric breakdown (sample E, pad g18). This cell shows saturation of the forward current ($I_{\text{max}} = 20.0 \text{ mA}$ at 3.2 V). [Similarly, pads g17 and g22 also show saturation ($I_{\text{max}} = 57 \text{ mA}$ at 3.4 V, and $I_{\text{max}} = 10 \text{ mA}$ at 4.4 V, respectively).]

decreasing in cycles 3–6, and the currents at maximum negative bias becoming more negative in cycles 2–6. Given the measured cross-sectional area of $50 \text{ \AA}^2 \text{ molecule}^{-1}$ (ref 3) and a pad area of 0.283 mm^2 , for cycle 1 the maximum forward current ($I = 4.08 \text{ mA}$ at 2.2 V) corresponds to a current of $4.51 \times 10^4 \text{ electrons molecule}^{-1} \text{ s}^{-1}$. The rectification ratio at 2.2 V is $RR = 4.08 \text{ mA}/0.759 \text{ mA} = 5.39$. The minimum nominal resistance is $2.2/0.004088 = 538 \Omega$ at 2.2 V and 2900Ω at -2.2 V .

The highest RR (27.5) was registered for cycle 1 of pad g3, shown in Figure 9: RR is then reduced to 10.1, 4.76, 2.44, and 1.86 in cycles 2–5, respectively. The data of Figure 9 are shown with the fit to eq 7. There is the slight hint of saturation of the current at positive bias (a decrease of slope in Figure 9 for $V > 2.0 \text{ V}$); a definite plateau at positive bias was not seen in any of the runs (but see below). Similar fits to eq 7 were obtained for all other runs for monolayers, as shown in Table 1. Satisfactory fits could also be obtained for monolayer data for $V > 0$ (or separately for $V < 0$) to eqs 2–5 (which have no plateau implied in the functional form), or to eq 6 (which implies

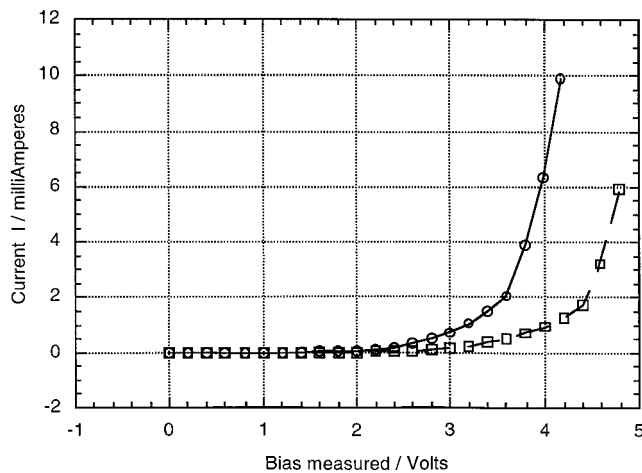


Figure 14. Current–voltage plots for the cell “Au pad|monolayer of $C_{16}H_{33}Q-3CNQ|Au$ base” (sample C, pad g16, cycles 2 and 2') driven until electrical breakdown: (a) circles, cell run from 0 V to 4.2 V with no breakdown ($I_{max} = 9.92$ mA at 4.2 V); (b) squares, same cell, run from 0 V until breakdown at 5.0 V ($I_{max} = 5.94$ mA at 4.8 V). Cell shows no saturation in the forward current. [Similarly, cells g15, g19, g20, and g21 show no saturation ($I_{max} = 1.56$ mA at 3.0 V, $I_{max} = 1.05$ mA at 3.4 V, $I_{max} = 0.0264$ mA at 4.8 V, and $I_{max} = 0.454$ mA at 7.6 V, respectively).]

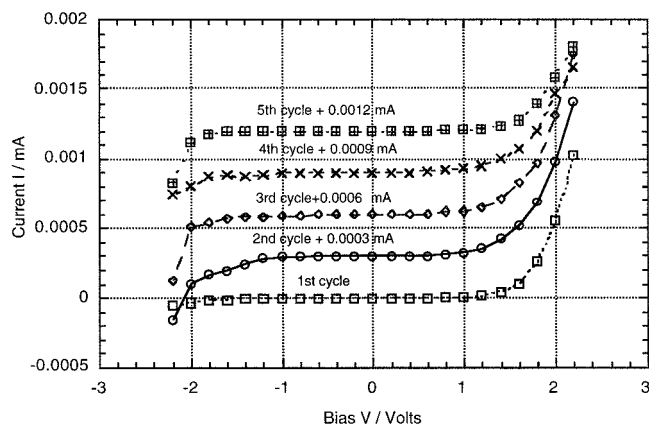


Figure 15. Current–voltage plots for five successive cycles of measurement for the same device, “Au pad|nine Z-type LB layers of $C_{16}H_{33}Q-3CNQ|Au$ base” (sample B, pad g25). For clarity, the data are displaced vertically upward by equal increments of 0.0003 mA for the successive cycles. The base is electrically grounded. At forward bias, positive current goes from the Au pad to the Au base (electrons flow from the Au base to the Au pad). Pad area = 0.283 mm². At 2.2 V in the first cycle, the resistance $R = 2.13$ M Ω , the current $I = 1.03$ μ A = 11.3 electrons molecule⁻¹ s⁻¹, and the rectification ratio RR = 19.70. RR decreases in successive cycles of measurement and disappears in cycle 6; RR becomes 2.42 (circles), 7.70 (diamonds), 4.84 (crosses), and 1.62 (crosses inside squares) in cycles 2–5, respectively.

a plateau). The fits for the data of Figure 9 to these equations are shown in Table 2. Figure 10 shows a logarithmic plot of the data in Figure 9: the asymmetry between forward and reverse bias for a monolayer of $C_{16}H_{33}Q-3CNQ$ is clear, when compared with Figure 7 for a monolayer of arachidic acid.

Figure 11 shows a full sweep for a monolayer of $C_{16}H_{33}Q-3CNQ$ between 3.0 and -3.0 V: there is some hysteresis and a rather large current at 3.0 V.

Figure 12 shows that the difference current between successive current–voltage sweeps has the same bias dependence as the original data.

Figures 13 and 14 show representative results for cells “Au|monolayer of $C_{16}H_{33}Q-3CNQ|Au$ ” measured by increasing the positive bias until dielectric breakdown occurs. Figure 13

shows the $I-V$ curve for pad g18, one of three pads (g17, g18, and g22) which definitely show a saturation in the current. In contrast, Figure 14 shows the $I-V$ curve for pad g16, one of the five pads (g15, g16, g25, g26, and g27) which show no saturation in the forward current, that is, no plateau. (When the cell breaks down, a current of 135 mA, limited by some protection circuit of the power supply, can be measured).

Figure 15 shows the electrical rectification by a nine-monolayer Z-type film of $C_{16}H_{33}Q-3CNQ$, sandwiched between Au electrodes. The currents are 3 orders of magnitude smaller than those for the monolayer, but the fits to the various equations are very similar, as is the decay of the rectification ratio with repeated cycles.

Discussion

Several conclusions can be drawn:

(1) Monolayer on Au. It is clear that the monolayer of **1** transferred with 100% efficiency from the air–water interface onto a Au substrate does not rearrange into locally folded multilayers: the measured thicknesses on Au or glass range from 2.24 nm (by ellipsometry) to 2.90 nm (X-ray diffraction). These measured values are consistent with the estimated molecular length of 3.0 nm;³ they also mirror previous findings on Al substrates.³ The only question is why the thickness from ellipsometry, which resembles the previous estimate by surface plasmon resonance,³ is shorter than the thickness by X-ray diffraction. This point will be examined again in more detail soon. It has relevance, because a 3.0-nm thick film implies that the molecules are stacked with all quinolinium rings eclipsing each other, while a 2.3-nm thick film implies that the aromatic part of the molecules is slanted³ with a 45° tilt to the normal to the surface, thus reducing the surface dipole moment. There is no evidence of monolayer folding to form ordered multilayers.

The grazing-angle infrared spectrum (Figure 2) is very similar to a previous spectrum measured on Al.³ The CN signals, which should have an intensity ratio of 2:1,³ are equally intense in the spectrum of Figure 2.

Naturally, we wonder what happens when the second Au electrode is evaporated as “cold gold” onto the monolayer. The cross section of the C_{16} chain is estimated to be about half that of the quinolinium ring, so it is possible that the first few Au atoms will penetrate partially in the spaces between the alkyl chains and will be stopped by the more compact aromatic part of the molecules. If the Au atoms are not stopped, then an electrical short circuit will occur, which we do observe for many pads. The measurements we show in Figures 6–15 are for those pads where no short circuit has occurred over an area of 0.283 mm². Since we cannot “peer under” the top Au pad, we cannot reassure a cynic that there is no folded multilayer under those pads that did not short, but the frequency of pads that are “good” in sample C (16 out of 48) speaks against this. Experts on ultrahigh vacuum spectroscopy may worry about how many monolayers of H₂O or N₂ may have deposited in our evaporator atop the coldfinger and before Au evaporation. But because low-pressure Ar gas is bled into the bell jar for 30 min before the sample support is cooled to 77 K, it may be presumed that Ar, and not H₂O, is the dominant species adsorbed atop the organic monolayer, as the thermalized Au atoms start to arrive. Presumably, Au slowly displaces the Ar atoms and ultimately forms a conducting pad.

(2) Origin of the Observed Rectification. It has been argued that previous observations of rectification in metal–monolayer–metal structures may have been due to contamination or other artifacts, unconnected to the specific electronic structure of the

TABLE 1: Current versus Voltage Data for C₁₆H₃₃Q–3CNQ, 1^a

pad (sample)	cycle	$V_{\max},^b$ V	$R@0.2$ V, ^c M Ω	$R@2.2$ V, ^d k Ω	RR@2.2 V ^e	$I@2.2$ V, ^f mA	fitting parameters to eq 7 ^g					
							I_0 , mA	E_0 , V	p	θ , V ⁻¹	r_p	
Monolayer Film												
g1(A)	1	2.2	0.007	0.538	5.39	4.09	0.039	1.31	0.37	4.52	0.999	
	2	2.2	0.009	0.526	4.52	4.19	0.0353	1.20	0.41	5.94	0.999	
	3	2.2	0.013	0.552	3.84	3.98	0.0311	1.14	0.43	7.41	0.999	
	4	2.2	0.019	0.635	3.16	3.46	0.0340	1.18	0.45	8.06	0.996	
	5	2.2	0.031	0.764	2.13	2.88	0.0278	1.13	0.47	8.61	0.997	
	6	2.2	0.045	1.38	1.24	1.60	0.0118	1.01	0.48	7.80	0.997	
g2(A)	1	2.2	0.121				0.00639	1.69	0.08	4.17	0.998	
	2	2.2	0.084	2.22		0.990	0.00743	1.32	0.33	6.52	0.998	
g3(C)	1	2.2	0.95	2.47	27.5	0.891	0.00642	1.61	0.21	9.64	0.999	
	2	2.2	2.2	6.10	10.1	0.361	0.00335	1.40	0.35	8.98	0.997	
	3	2.2	6.7	14.4	4.76	0.152	0.00111	1.14	0.42	8.51	0.995	
		2.2	10	26.6	2.44	0.083	0.00061	1.08	0.46	9.60	0.997	
		2.2	20	35.8	1.86	0.062	0.00046	1.06	0.47	9.51	0.997	
g4(C)	1	2.2	1.5	4.09	12.7	0.538	0.00447	1.27	0.40	14.85	0.999	
	2	2.2	1.3	4.39	5.16	0.501	0.00443	1.16	0.46	14.19	0.998	
g5(C)	1	2.2	2.9	14.6	4.36	0.152	0.00115	1.13	0.44	10.48	0.998	
	3	2.2	0.77	2.53	9.69	0.869	0.00600	1.17	0.42	14.05	0.999	
g6(C)	1	2.2	5.0	16.2	2.11	0.136	0.0010	1.08	0.47	10.61	0.997	
g7(C)	1	2.2	0.004	0.068	0.95	32.5	0.507	1.31	0.41	8.15	0.995	
		2.2	0.006	0.142	3.27	15.5	0.132	1.13	0.42	7.54	0.996	
g8(C)	1	2.2	0.020	0.222	3.32	9.88	0.0774	1.11	0.44	7.76	0.997	
	2	2.2	0.043	0.345	2.28	6.37	0.0498	1.08	0.46	9.52	0.997	
g9(C)	1	2.2	4.0	19.4	8.86	0.113	0.000783	1.17	0.39	8.60	0.999	
	2	2.2	4.0	28.3	5.34	0.078	0.000596	1.17	0.42	8.27	0.997	
g10(C)	1	2.2	0.012	0.159	17.99	13.86	0.116	1.60	0.19	4.86	0.998	
	2	2.2	0.039	0.357	6.53	6.16	0.0458	1.15	0.42	9.96	0.999	
g11(C)	1	2.2	0.017	0.408	6.68	5.39	0.0426	1.20	0.40	7.36	0.999	
	2	2.2	0.023	0.369	4.54	5.97	0.0454	1.12	0.44	9.16	0.999	
	3	2.2	0.052	0.65	2.63	3.38	0.0355	1.15	0.47	9.24	0.996	
g12(C)	1	2.2	0.161	1.66	10.81	1.32	0.00981	1.40	0.30	6.21	0.997	
	2	2.2	0.741	3.58	1.46	0.614	0.00433	1.04	0.48	13.44	0.999	
g13(C)	1	2.2	0.014	0.297	5.13	7.41	0.0591	1.17	0.42	7.12	0.998	
	2	2.2	0.054	0.585	3.31	3.76	0.0377	1.16	0.46	10.59	0.997	
g14(C)	1	2.2	20	507	2.50	0.0434	0.000319	1.08	0.47	11.22	0.996	
	2	2.2	20	110	0.86	0.0199	0.000166	1.01	0.51	10.59	0.997	
g15(C)	1	3.0	20	45.8		0.048						
g16(C)	2	4.2	0.46	19.7		0.114						
	2'	4.8	3.3	0.063		0.035						
g17(C)	3	3.4	0.051	0.075		0.035						
g18(E)	1	3.2	0.084	0.405		5.42						
g19(E)	1	5.8		43.4		0.0507						
g20(E)	1	4.8		7333.0		0.00030						
g21(E)	1	7.6	200	3960		0.00057						
g22(E)	1	4.4	20.0	39.7		0.0554						
g23(C)	1	2.2	23.8	27.1	1.30	0.081	0.00596	1.42	0.46	17.29	0.998	
	2	3.0		149	0.33	0.015	0.00611	1.56	0.48	17.27	0.990	
g24(C)	1	3.2	0.057	0.268	6.62	8.20	0.438	1.52	0.45	10.08	0.997	
							0.500	1.63	0.47	8.39	0.997	
	2	3.2	0.392	0.423	4.59	5.20	0.296	1.51	0.47	12.82	0.993	
							0.619	1.72	0.47	9.77	0.995	
Nine-Layer Film												
g25(B)	1	2.2	1.0×10^3	2.1×10^3	19.70	0.00103						
	2	2.2	1.0×10^3	2.0×10^3	2.42	0.00110	8.0×10^{-6}	1.07	0.46	10.04	0.995	
	3	2.2	6.7×10^2	1.9×10^3	7.70	0.00115	7.7×10^{-6}	1.06	0.46	13.28	0.989	
	4	2.2	6.7×10^2	2.9×10^3	4.84	0.00076	5.2×10^{-6}	1.11	0.42	9.33	0.997	
	5	2.2	6.7×10^2	3.6×10^3	1.62	0.00060	3.9×10^{-6}	1.04	0.47	17.39	0.991	
g26(B)	1	2.2	4.0×10^2	1.13×10^3	4.34	0.00196	1.4×10^{-5}	1.11	0.46	16.24	0.996	
	2	2.2	4.0×10^2	2.63×10^3	1.07	0.00084	5.9×10^{-6}	1.03	0.49	15.85	0.992	
	3	2.2	2.9×10^2	1.67×10^3	0.85	0.00132	1.0×10^{-5}	1.03	0.49	15.27	0.989	

^a All runs used monolayers of C₁₆H₃₃Q–3CNQ, except for runs g25 and g26 (for nine Z-type layers of C₁₆H₃₃Q–3CNQ). Almost all runs used $V_{\max} = 2.2$ V. The exceptions are pads g23 and g21 ($V_{\max} = 3.0$ or 3.2 V), and pads g15, g16, and g17, for which data were collected from $V = 0$ until breakdown (the listed V_{\max} is the maximum before a short circuit). The average parameter values (using only the monolayer data and only the first cycle) are (RR) = 7.55, (E_0) = 1.32 V, (p) = 0.37, and (θ) = 9.16 V⁻¹. Runs g17, g19, and g22 (underlined), when driven to breakdown, show plateaus in the current, while runs g15, g16, g19, g20, and g21 do not. ^b Maximum bias used. ^c Ohm's law resistance R at 0.2 V bias. ^d Ohm's law resistance R at 2.2 V bias. ^e Rectification ratio RR at 2.2 V bias (eq 1). ^f Current I at 2.2 V bias. ^g Fits to eq 7 in the parametrized form: $I = a\{\tan^{-1}[\theta E_0 + \theta p V] - \tan^{-1}[\theta E_0 - \theta V + \theta p V]\}$. Here a is current amplitude (mA), \tan^{-1} values are given in radians, E_0 is the difference between the energy of the molecular orbital involved in the electron transfer and the Fermi level of the grounded electrode (both relative to the vacuum level), p is the fractional distance of the center of gravity of the electroactive part of the molecule from the grounded electrode, θ is a tunneling gap parameter, and r_p is Pearson's r factor,³² determined by Marquandt's algorithm (with preceding zero if $100r_p < 99\%$).

TABLE 2: Fit of Data of Figure 9 to the Theoretical Equations $I = a \exp(bV)$ [Eq 2], $I = a' \exp(b'V^{0.5})$ [Eq 3], $I = a'' \exp(b''V^{0.25})$ [Eq 4], $I = a'''V^{0.5} \exp(-b'''V^{0.5})$ [Eq 5], and $I = a''''\{\tan^{-1}[b''''(c + V)] - \tan^{-1}[b''''(c - V)]\}$ [Eq 6], with Pearson's Index of Fit r_p

eq	parameters	$a, a', a''',$ or a''''	$b, b', b''',$ or b''''	c''''	r_p
2	a, b	$(2.92 \pm 0.83) \times 10^{-4}$	$(3.65 \pm 0.13) \times 10^{-4}$		0.9983
3	a', b'	$(2.11 \pm 1.18) \times 10^{-7}$	10.29 ± 0.38		0.9983
4	a'', b''	$(1.04 \pm 0.12) \times 10^{-13}$	24.45 ± 0.93		0.9983
5	a''', b'''	$(4.08 \pm 2.29) \times 10^{-7}$	-9.58 ± 0.38		0.9983
6	a'''', b'''', c	$(3.59 \pm 0.08) \times 10^{-1}$	8.04 ± 0.44	2.030 ± 0.007	0.9995

deposited molecules. However, no rectification is seen with monolayers of arachidic acid ($n\text{-C}_{19}\text{H}_{39}\text{COOH}$) (Figures 5 and 6), as expected: an RR marginally greater than 1.0 is a negligible asymmetry in the current.⁴ The capacitance of the layer causes the slight hysteresis in the I - V cycles of Figures 5 and 6. The log I versus V plot (Figure 7) is linear with V beyond 1 V and is roughly symmetrical between positive and negative bias.

(3) Conducting Defects in LB Films. Until the work of Okazaki and Sambles,³¹ all metal-monolayer-metal cells with noble metal top contacts were inevitably short-circuited by penetrating nanofilaments. Normally, when a metal is evaporated onto a monolayer, the monolayer is heated both directly by contact with the hot metal vapor and indirectly by radiation and conduction from the evaporation source. While this heating has long been suspected of causing damage, attempts to avoid it, by mounting the substrate on a coldfinger, have not been successful for work with gold. This is consistent with the structural defects being too soft to withstand the wetting forces during the initial stages of evaporation. The surface energy of gold is approximately 1 N m^{-1} , more than an order of magnitude higher than that of any molecular material. Okazaki and Sambles' result³¹ suggests that wetting forces alone do not convert the structural defects, known to be present, into conducting defects. The present evaporation configuration was inspired by, but was not a slavish copy of, that of Okazaki and Sambles.³¹ In analogy to the use of a coldfinger, our procedure avoids heating of the monolayer by conductive heating. Additionally, it avoids contact of the monolayer with hot vapor or with radiation from the evaporation source. The reasonable yield of non-short-circuited cells in the present study confirms that the latter two sources of monolayer heating have been a major cause of cell failure in previous work. A mechanism is now known by which heating can convert structural defects into conducting defects. Many monolayers undergo a cooperative phase transition on heating, which proceeds by the topological growth of line defects characteristic of the high-temperature phase.³⁴ The birefringence, observed in metal films evaporated onto LB films, results from the alignment along these line defects of the metallic nanoparticles formed during the initial phases of evaporation.³³ The present success is consistent with a picture in which the initial structural defects are points of weakness and at which the line defects nucleate and subsequently destroy the lamellar integrity of the monolayer. It should be noted that the present evaporation configuration absolutely requires the use of a contact mask to define the metal islands of the top contacts, as the evaporated gold no longer travels in straight lines. As LB films are in general extremely soft, this introduces the possibility of mechanical damage. We have avoided this by coating the mask with a thin layer of hydrophobic elastomer.

(4) Rectification. The electrical rectification by LB monolayers of $\text{C}_{16}\text{H}_{33}\text{Q}-3\text{CNQ}$, first reported 10 years ago between unsymmetrical electrodes¹ and confirmed between symmetrical Al pads three years ago,³ is now confirmed again (Figures

8–14), this time between oxide-free Au electrodes, and it is definitely molecular in origin. The currents through a Au pad of macroscopic dimensions are large, because most molecules under the Au pad can now be involved in the rectification. (There is no oxide in the way!) The maximum forward currents measured at 2.2 V for an LB monolayer of $\text{C}_{16}\text{H}_{33}\text{Q}-3\text{CNQ}$ between Au electrodes are 4.5×10^4 electrons molecule⁻¹ s⁻¹ (Figure 8), 9.83×10^3 electrons molecule⁻¹ s⁻¹ (Figure 9), and 9.04×10^4 electrons molecule⁻¹ s⁻¹ (Figure 11). These currents are much larger than the current values of 0.33 electrons molecule⁻¹ s⁻¹ previously reported between Al electrodes (with their partial oxide covering)³ and 35 electrons molecule⁻¹ s⁻¹ reported for an improved Al electrode design.³⁵ These currents are also 2 orders of magnitude larger than the values of 138 electrons molecule⁻¹ s⁻¹ (Figure 5) and 84.3 (Figure 6) electrons molecule⁻¹ s⁻¹ measured for a monolayer of the saturated alkane carboxylic acid, arachidic acid, $\text{C}_{19}\text{H}_{39}\text{COOH}$. The maximum rectification ratio for $\text{C}_{16}\text{H}_{33}\text{Q}-3\text{CNQ}$ at ± 2.2 V was 27.5 (Figure 9); the average was 7.55 (Table 1). The currents decrease during successive cycles (Figure 8), and the rectification ratios become smaller, as the molecules presumably reorient in the monolayer;³ this may be related to the damage known to occur in monolayers of long aliphatic chains because of the passage of hot electrons.³⁶ One should consider the possibility of chemical degradation. The first reduction of $\text{C}_{16}\text{H}_{33}\text{Q}-3\text{CNQ}$ is electrochemically reversible in solution,³ so no damage occurs by adding one electron to the LUMO (which is concentrated on the 3CNQ part of the molecule);⁶ oxidizing the molecule in solution is electrochemically not reversible.³ The large current at negative bias in the last cycle of Figure 8 suggests that the number of molecules conducting is not decreasing dramatically as the cycles proceed; therefore, the molecular reorientation mentioned above is more likely. Furthermore, Figure 12 shows that the difference between the currents measured in successive bias sweeps exhibits the same qualitative dependence on bias as do the original data: this also suggests that there is a gradual reorientation of the molecules in the monolayer. This reorientation may be preventable if a polymerizable monolayer, or a monolayer covalently attached to a surface by "self-assembly", were available. The log I versus V curve (Figure 10) is no longer symmetrical between positive and negative bias.

(5) Multilayers of $\text{C}_{16}\text{H}_{33}\text{Q}-3\text{CNQ}$ show rectification with RR as high as 19.2 (Figure 15), but the currents (11.3 electrons molecule⁻¹ s⁻¹) are smaller by 3 orders of magnitude than those for the monolayer, because the current must cross the several insulating hexadecyl tails required for LB assembly.

(6) Saturation of Current at High Voltages. Some effort was made to fit the measured data to theoretical equations that have been used to discuss conductivity or tunneling in thin films. As discussed in the captions to Figure 9 and Table 2, the data (particularly if divided into $V < 0$ and $V > 0$ subsets) can be fitted well to eqs 2–6. A fit for all V to eq 7 was quite satisfactory for most data sets (Table 1). The issue of what a theoretical rectification curve should look like must now be discussed. If only elastic processes are considered, then the

spectrum of the current should be approximately a Lorentzian function of the voltage, as calculated by Hall et al.²⁶ or by Peterson et al.²⁷ When the dominant level lies between the Fermi levels of the two electrodes, which occurs for sufficiently high voltage of either sign, the current saturates. Current saturation is also a prediction of the computer model of Aviram and Ratner,³⁷ which additionally involves inelastic mechanisms. We therefore sought evidence for a “plateau” in the I - V curves. When the maximum bias is set at 2.2 V (Figures 8–10), one barely sees a reduction of the slope between 2.0 and 2.2 V. Some cells were pushed to higher voltages, until breakdown occurred (Figures 13 and 14). It should be remembered that the monolayer thickness is only 2.3–2.9 nm, so 2.3 V across it means an impressively large electric field of up to 1 GV m⁻¹! Two distinct phenomena occurred: some cells showed saturation in the forward current (Figure 13), and some did not (Figure 14). It is very likely that Au atoms can migrate at these higher potentials from the bottom electrode or, more likely, from the top electrode, to occupy voids in the monolayer, for example, between adjacent alkyl chains; this effect has been seen for LB multilayers.³⁸ If the Au atoms migrate until breakdown occurs, then we see the situation shown in Figure 14. If, on the contrary, the Au atoms do not migrate or stop migrating, and if the zwitterionic chromophore is therefore left intact, then the situation of Figure 13 will occur: a definite plateau is seen, as predicted either by the Aviram–Ratner model or by eq 7.

(7) Relevant Molecular Energy Level. The bias at which enhanced electron flow occurs can be estimated from Figure 9 to be around 1.6 V. The fits of the data to eq 7b, shown in Table 1, suggest that the LUMO level of C₁₆H₃₃Q–3CNQ, which may be responsible for the rectification, is $\langle E_0 \rangle = 1.32 \pm 0.25$ eV above $E_F(\text{Au})$, the Fermi level of Au. If we take $E_F(\text{Au}) = -5.3$ eV, then the LUMO energy of C₁₆H₃₃Q–3CNQ is at -4.0 ± 0.25 eV, relative to the vacuum level. From the bias at which enhanced electron flow occurs, our previous work with Al electrodes found $1.0 < E_0 < 1.3$ V relative to $E_F(\text{Al})$:³ using $E_F(\text{Al}) = -4.2$ eV, the LUMO is placed between -2.9 and -3.3 eV from the vacuum level,³ which is 0.45–1.35 eV higher than the estimate made here with Au electrodes. One should also remember that the Aviram–Ratner model³⁷ involves the HOMO as well as the LUMO.

(8) Centering of the Relevant Molecular Energy Level within the Electrode Gap. Equation 7 has a parameter $\langle p \rangle$, which estimates, in a “lever-rule” argument, the fractional position of the dominant molecular orbital between the two metal electrodes (Figure 4). The result, $\langle p \rangle = 0.37 \pm 0.11$, argues that the relevant orbital is somewhere in the aromatic part of the molecule. Only the LUMO is consistent with the observed direction of easy current flow. If the estimated molecular length is 3 nm, the aromatic part is 1 nm long, the quinolinium ring is 0.4 nm long, and the 3CNQ part is 0.6 nm long, and if the LUMO is localized on the 3CNQ part,⁶ then $p = (1/2)0.6/3.0 = 0.10$. If the orbital is spread through the aromatic part, then $p = (1/2)(1.0/3.0) = 0.16$; if the orbital is centered on the quinolinium ring, then $p = 0.8/3.0 = 0.27$. EPR data suggest that the LUMO is centered on the 3CNQ part of the molecule,⁶ which would argue for $p = 0.10$. The disagreement between $\langle p \rangle = 0.37 \pm 0.11$ and $p = 0.10$ may be because eq 7 is a fairly simple model for the conductivity.

(9) Direction of Enhanced Conductivity. The direction of larger conductivity in the forward direction agrees with what was previously established with monolayers of C₁₆H₃₃Q–3CNQ sandwiched between Al electrodes,³ and therefore with a modification³ of the Aviram–Ratner model:³⁷ electrons move

(Figure 3) from the bottom pad, through the dicyanomethylene end of the molecule and then through the quinolinium end, to the top pad.

(10) Theoretical Calculations. A recent theoretical calculation³⁹ predicts enhanced currents in the direction opposite to our previous³ observation for Al electrodes and emphasizes that the electrical asymmetry is strongly enhanced by an asymmetric placement of the zwitterionic chromophore within the monolayer (i.e., current would become symmetric if there were no C₁₆H₃₃ tail).³⁹ An older calculation polarizes the molecule in extremely high fields and again predicts currents in a direction opposite to observation.⁴⁰ There is an older calculation,⁴¹ and also a more recent one,⁴² which does not discuss the transport problem. We must conclude that further theoretical studies are needed.

Conclusion

We have established again, this time with oxide-free Au electrodes, that the zwitterionic molecule C₁₆H₃₃Q–3CNQ is a rectifier of electrical current as a single monolayer. The currents measured are as large as 9.04×10^4 electrons molecule⁻¹ s⁻¹ at a 2.2 V forward bias. The data, coupled with a theoretical equation, allow us to make an estimate that the relevant molecular orbital for enhanced electron transfer is at -4.0 ± 0.25 eV, relative to vacuum. We have also established saturation of the forward current at high bias.

Acknowledgment. We thank DOE-EPSCoR (DE-FC02-91-ER-75678) for financial support. We also thank Mr. Jeffrey W. Baldwin for the FTIR spectrum of Figure 2.

References and Notes

- (1) Ashwell, G. J.; Sambles, J. R.; Martin, A. S.; Parker, W. G.; Szablewski, M. Rectifying Characteristics of Mg | (C₁₆H₃₃-Q3CNQ LB Film) | Pt Structures. *J. Chem. Soc., Chem. Commun.* **1990**, 1374–1376.
- (2) Martin, A. S.; Sambles, J. R.; Ashwell, G. J. Molecular Rectifier. *Phys. Rev. Lett.* **1993**, *70*, 218–221.
- (3) Metzger, R. M.; Chen, B.; Höpfner, U.; Lakshmikantham, M. V.; Vuillaume, D.; Kawai, T.; Wu, X.; Tachibana, H.; Hughes, T. V.; Sakurai, H.; Baldwin, J. W.; Hosch, C.; Cava, M. P.; Brehmer, L.; Ashwell, G. J. Unimolecular Electrical Rectification in Hexadecylquinolinium Tricyanoquinodimethanide. *J. Am. Chem. Soc.* **1997**, *119*, 10455.
- (4) Vuillaume, D.; Chen, B.; Metzger, R. M. Electron Transfer through a Monolayer of Hexadecylquinolinium Tricyanoquinodimethanide. *Langmuir* **1999**, *15*, 4011–4017.
- (5) Chen, B.; Metzger, R. M. Rectification between 370 K and 105 K in Hexadecylquinolinium Tricyanoquinodimethanide. *J. Phys. Chem. B* **1999**, *103*, 4447–4451.
- (6) Baldwin, J. W.; Chen, B.; Street, S. C.; Konovalov, V. V.; Sakurai, H.; Hughes, T. V.; Simpson, C. S.; Lakshmikantham, M. V.; Cava, M. P.; Kispert, L. D.; Metzger, R. M. Spectroscopic Studies of Hexadecylquinolinium Tricyanoquinodimethanide. *J. Phys. Chem. B* **1999**, *103* (21), 4269–4277.
- (7) Metzger, R. M. Demonstration of Unimolecular Electrical Rectification in Hexadecylquinolinium Tricyanoquinodimethanide. *Adv. Mater. Opt. Electron.* **1998**, *8*, 229–245.
- (8) Metzger, R. M.; Cava, M. P. Rectification by a Single Molecule of Hexadecylquinolinium Tricyanoquinodimethanide. *Ann. N.Y. Acad. Sci.* **1998**, *852*, 95–115.
- (9) Metzger, R. M. Unimolecular Electrical Rectification by Hexadecylquinolinium Tricyanoquinodimethanide. *Mol. Cryst. Liq. Cryst.* **1999**, *337*, 37–42.
- (10) Metzger, R. M. Unimolecular Rectification down to 105 K and Spectroscopy of Hexadecylquinolinium Tricyanoquinodimethanide. *Synth. Met.* **2000**, *109*, 23–28.
- (11) Metzger, R. M.; Chen, B.; Vuillaume, D.; Lakshmikantham, M. V.; Höpfner, U.; Kawai, T.; Baldwin, J. W.; Wu, X.; Tachibana, H.; Cava, M. P. Observation of Unimolecular Electrical Rectification in Hexadecylquinolinium Tricyanoquinodimethanide. *Thin Solid Films* **1998**, *327–329*, 326–330.
- (12) Metzger, R. M.; Chen, B.; Vuillaume, D.; Höpfner, U.; Baldwin, J. W.; Kawai, T.; Tachibana, H.; Sakurai, H.; Lakshmikantham, M. V.; Cava, M. P. Electrical Rectification by a Molecule of Hexadecylquinolinium Tricyanoquinodimethanide. In *Electrical, Optical, and Magnetic Properties*

of *Organic Solid-State Materials*; Chiang, L. Y., Dalton, L. R., Jen, A. Y., Reynolds, J., Rubner, M., Eds.; Materials Research Society: Pittsburgh, PA, 1998; Vol. 488, pp 335–340.

(13) Metzger, R. M. The Unimolecular Rectifier: Unimolecular Electronic Devices Are Coming. *J. Mater. Chem.* **1999**, *9*, 2027–2036.

(14) Metzger, R. M. Electrical Rectification by a Molecule: The Advent of Unimolecular Electronic Devices. *Acc. Chem. Res.* **1999**, *32*, 950–957.

(15) Metzger, R. M. All About γ -Hexadecylquinolinium Tricyanoquinodimethanide, a Unimolecular Rectifier of Electrical Current. *J. Mater. Chem.* **2000**, *10*, 55–62.

(16) Xu, T.; Peterson, I. R.; Lakshmikantham, M. V.; Metzger, R. M. Rectification by a Monolayer of Hexadecylquinolinium Tricyanoquinodimethanide between Gold Electrodes. *Angew. Chem., Int. Ed. Engl.* **2001**, *40*, 1749–1752.

(17) Sommerfeld, A.; Bethe, H. In *Handbuch der Physik*; Geiger, H., Scheel, K., Eds.; Springer: Berlin, 1933; Vol. 24, p 430.

(18) Mann, B.; Kuhn, H. Tunneling through Fatty Acid Salt Monolayers. *J. Appl. Phys.* **1971**, *42*, 4398–4405.

(19) Roberts, G. G.; Vincett, P. S.; Barlow, W. A. AC and DC Conduction in Fatty Acid Langmuir Films. *J. Phys.* **1978**, *C11*, 2077–2085.

(20) Tredgold, R. H.; Winter, C. S. Tunneling Currents in Langmuir–Blodgett Monolayers of Stearic Acid. *J. Phys. D* **1981**, *14*, L185–L188.

(21) Hao, S.; Blott, B. H.; Melville, D. Metal Langmuir–Blodgett Metal Junctions Using Pb–In Superconducting Electrodes. *Thin Solid Films* **1985**, *135*, 63–68.

(22) Peterson, I. R. A Structural Study of the Conducting Defects in Fatty-Acid Langmuir–Blodgett Films. *J. Mol. Electron.* **1986**, *2*, 95–99.

(23) Simmons, J. G. Poole-Frenkel Effect and Schottky Effect in Metal-Insulator-Metal Systems. *Phys. Rev.* **1967**, *155*, 657–660.

(24) Landauer, R. Spatial Variation of Currents and Fields due to Localized Scatterers in Metallic Conduction. *IBM J. Res. Dev.* **1957**, *1*, 223–231.

(25) Datta, S. *Electronic Transport in Mesoscopic Systems*; Cambridge University Press: Cambridge, U.K., 1995.

(26) Hall, L. E.; Reimers, J. R.; Hush, N. S.; Silverbrook, K. Formalism, Analytical Model, and a Priori Green's-function-based Calculations of the Current–Voltage Characteristics of Molecular Wires. *J. Chem. Phys.* **2000**, *112*, 1510–1521.

(27) Peterson, I. R.; Vuillaume, D.; Metzger, R. M. An Analytical Model for Molecular-scale Charge Transport. *J. Phys. Chem. A* **2001**, *105*, 4702–4704.

(28) Metzger, R. M.; Chen, B. Unimolecular Organic Rectifier of Electrical Current, U.S. Patent 6,169,291, January 2, 2001.

(29) Solina, D. M.; Cheary, R. W.; Swift, P. D.; Dligatch, S.; McCredie, G. M.; Gong, B.; Lynch, P. Investigation of the Interfacial Structure of Ultrathin Platinum Films Using X-ray Reflectivity and X-ray Photoelectron Spectroscopy. *Thin Solid Films* **2000**, *372*, 94–103.

(30) Warren, B. E. *X-ray Diffraction*; Addison-Wesley: Reading, MA, 1969; pp 251–254.

(31) Okazaki, N.; Sambles, J. R. A New Fabrication Technique and Current–Voltage Properties of a Au/LB/Au Structure. In *Extended Abstracts, International Symposium on Organic Molecular Electronics*, Nagoya, Japan, 18–19 May 2000; pp 66–67.

(32) Pearson, K. *Philos. Mag.* **1900**, *50*, 157–172.

(33) Peterson, I. R.; Russell, G. J.; Earls, J. D.; Sambles, J. R. Birefringence Effects in Metal Overlayers on Langmuir–Blodgett Films. *Thin Solid Films* **1987**, *150*, 83–88.

(34) Merle, H. J.; Steitz, R.; Pietsch, V.; Peterson, I. R. The Lamellar–Columnar Transition in Langmuir–Blodgett Multilayers of Cadmium Soaps. *Thin Solid Films* **1994**, *237*, 236–245.

(35) Metzger, R. M. Unimolecular Rectification Down to 105 K and Spectroscopic Properties of Hexadecylquinolinium Tricyanoquinodimethanide. *Mater. Res. Soc. Symp. Proc.*, in press (MRS Paper H12.2).

(36) Steitz, R.; Peterson, I. R. In *Electron Crystallography of Organic Molecules*; Fryer, J. R., Dorset, D. L., Eds.; NATO ASI C378; Kluwer: Dordrecht, Holland, 1990; pp 365–375.

(37) Aviram, A.; Ratner, M. A. Molecular Rectifiers. *Chem. Phys. Lett.* **1974**, *29*, 277–283.

(38) Couch, N. R.; Montgomery, C. M.; Jones, R. Metallic Conduction through Langmuir–Blodgett Films. *Thin Solid Films* **1986**, *135*, 173–182.

(39) Krzeminski, C.; Delerue, C.; Allan, G.; Vuillaume, D.; Metzger, R. M. Theory of Electrical Rectification in a Molecular Monolayer. Manuscript in preparation.

(40) Pickholz, M.; dos Santos, M. C. AM1/CI Study of a Molecular Rectifier. *THEOCHEM* **1998**, *432*, 89–96.

(41) Broo, A.; Zerner, M. C. Electronic Structure of Donor–Spacer–Acceptor Molecules of Potential Interest for Molecular Electronics. IV. Geometry and Device Properties of P3CNQ and Q3CNQ. *Chem. Phys.* **1995**, *196*, 423–436.

(42) Kwon, O.; McKee, M. L.; Metzger, R. M. Theoretical Calculations of Methylquinolinium Tricyanoquinodimethanide (CH₃Q–3CNQ) Using a Solvation Model. *Chem. Phys. Lett.* **1999**, *313* (1,2), 321–331.